ACS SENSORS

pubs.acs.org/acssensors

Article

μPADs on Centrifugal Microfluidic Discs for Rapid Sample-to-Answer Salivary Diagnostics

Shixian Liu, Yuting Hou, Zirui Li, Chenyu Yang, and Guozhen Liu*

Cite This: ACS Sens. 2023, 8, 3520−3529

Read Online

ACCESS | Metrics & More | Article Recommendations | Supporting Information

ABSTRACT: A fully integrated device for salivary detection with a sample-in-answer-out fashion is critical for noninvasive point-of-care testing (POCT), especially for the screening of contagious disease infection. Microfluidic paper-based analytical devices (μPADs) have demonstrated their huge potential in POCT due to their low cost and easy adaptation with other components. This study developed a generic POCT platform by integrating a centrifugal microfluidic disc with μPADs to realize sample-to-answer salivary diagnostics. Specifically, a custom centrifugal microfluidic disc integrated with μPADs is fabricated, which demonstrated a high efficiency in saliva treatment. To demonstrate the capability of the integrated device for salivary analysis, the SARS-CoV-2 Nucleocapsid (N) protein, a reliable biomarker for SARS-CoV-2 acute infection, is used as the model analyte. By the chemical treatment of the μPAD surface, and by optimizing the protein immobilization conditions, the on-disc μPADs were able to detect the SARS-CoV-2 N protein down to 10 pg mL^{-1} with a dynamic range of 10−1000 pg mL^{-1} and an assay time of 8 min. The integrated device was successfully used for the quantification of the N protein of pseudovirus in saliva with high specificity and demonstrated a comparable performance to the commercial paper lateral flow assay test strips.

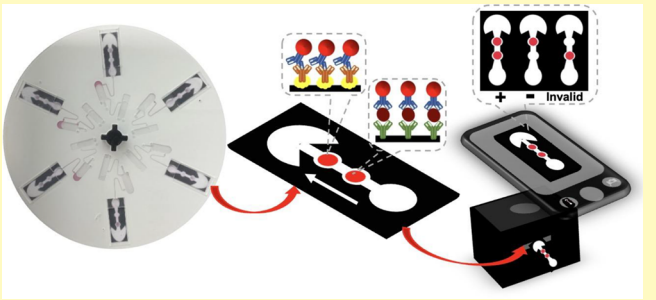

KEYWORDS: *microfluidic paper-based analytical devices, centrifugal microfluidic disc, salivary diagnostics, SARS-CoV-2, point-of-care testing*

Saliva is a complex matrix that reflects the hormonal, immunological, metabolic, and nutritional state of the body. It is considered to be the most appropriate biological fluid for scientific investigations in the diagnosis, prognosis, and surveillance of diseases, alongside the noninvasive and ease of collection properties.[1] Many studies report diseases signaling salivary biomarkers for local or systemic pathologies like oral cancer, endocrine and immunologic pathologies, infectious and neurological diseases, and so forth.[2] The successful rapid screening of salivary severe acute respiratory syndrome coronavirus 2 (SARS-CoV-2) infection has further highlighted the importance of saliva in convenient/noninvasive point-of-care testing (POCT). The need for fast, cost-effective, and reliable methods for saliva investigation has led to high technological advances in developing sensing tools.[3] In most cases, accurate salivary diagnostics still require a multiple-step process to alleviate the matrix effects and interferences.[4,5] However, the complex matrix with its non-Newtonian behavior and high viscosity poses handling challenges. Several tedious and long preanalytical steps, incompatible with the point-of-need use, are required to liquefy and homogenize saliva samples before protein analysis can be performed.[6]

Centrifugal microfluidics provide a lab-on-a-disc platform for efficient biochemical analysis due to the simplicity, small size, portability, low cost, and adaptability to various POCT assays.[7,8] Centrifugal microfluidics also play an important role in the matrix sample preparation individually or in integrated devices. Harrison and co-workers developed a centrifugal microfluidic disc performing sample cleanup on human serum samples for metabolite analysis.[9] Veres and co-workers reported an on-chip nucleic acid extraction assay to separate plasma from a whole blood sample using a centrifugal microfluidic platform, allowing for pneumatic actuation of liquids during rotation. Recently, they integrated RNA extraction with the active pneumatic pumping and developed an automated sample-to-answer centrifugal microfluidic system for rapid molecular diagnostics of SARS-CoV-2 with the sensitivity of 0.5 copies per microliter, which is highly competitive to quantitative reverse transcriptase polymerase chain reaction (RT-qPCR).[10] Lander's group developed a rapid, simple centrifugal microfluidic device for the isolation of SARS-CoV-2 RNA that could prepare six samples within 15

Received: May 30, 2023
Accepted: August 22, 2023
Published: September 5, 2023

min. However, mixing the sample and nanoparticles was conducted off-disc, leading to a reduced automation of the setup.[11] To conquer the challenges of salivary diagnostics, Mitsakakis' group introduced a magnet-beating method to realize liquefaction and homogenization for POC protein analysis.[12] This system requires the insertion of a magnet bar into the sample chamber and the setting of several external permanent magnets, which result in increased costs and equipment complexity.

Providing reliable, speedy, early disease diagnosis and timely treatment are critical and essential for restraining the virus spread, such as SARS-CoV-2.[13,14] RT-qPCR and high-throughput gene sequencing on the nasal and pharyngeal swab specimens are the popular methods for the early diagnosis of SARS-CoV-2.[15] These molecular tests are highly sensitive and specific at detecting viral RNA and are recommended by WHO for confirming the diagnosis in individuals who develop clinical symptoms.[16] However, these clinical and conventional approaches require expensive instruments, trained personnel, and close contact between healthcare workers and patients, posing a risk of transmission of the virus and causing discomfort or bleeding. Hence, nasopharyngeal or oropharyngeal swabs are not desirable for the sequential monitoring of the viral load. The collection of saliva is noninvasive and greatly minimizes the exposure of healthcare workers to the virus. Saliva has a high consistency rate of greater than 90% with nasopharyngeal specimens in the detection of respiratory viruses, including coronaviruses.[17] Therefore, the development of POCT being reliable, sensitive, selective, portable, and cost-effective for salivary diagnostics has gained extensive attention in contagious virus screening.

As the most popular POCT platform, paper-based lateral flow assay (LFA) has been widely used for screening COVID-19 infection by the detection of virus antibodies IgG and IgM, and also virus proteins, although it is less sensitive than molecular tests.[18,19] As a result, nitrocellulose (NC) membrane, one of the most important raw materials for making LFA test strips, is in high market demand, leading to short supply and super-high price. Additionally, NC membranes are hydrophobic, flammable, and toxic and might cause environmental concerns.[20] Filter paper is a cellulosic material that has many unique and excellent properties for fabricating biosensors, such as low cost (a simple μPAD typically can be manufactured for under $0.01) and rich surface chemistry. Cellulosic paper shows chiral structures at many levels, from the chirality inherent in each sugar unit to chiral interactions between nanocrystals, chiral twisting of microfibrils, and helical organization of microfibrils in plant cell walls, which can be modified with various functional groups to introduce proteins, DNA, or small molecules. Further, the porous structure of cellulosic paper provides a high surface-to-volume ratio and increases the number of biomolecules to be immobilized, leading to improved detection sensitivity.[21] Its high flexibility and deformability facilitate the complex 3D structural formation and accommodate different printing techniques.[22] The unique characteristics of cellulosic paper are its ecofriendly nature with easy decomposition, impressive biocompatibility, and potential to provide a strong contrast to a colored substrate.[23] Compared with LFA, μPADs demonstrate superior performance in quantitative analysis with various signal readout formats such as colorimetric techniques, chemiluminescence, electrochemiluminescence, fluorescence, and electrochemistry.[24−26] Recently, we have developed μPADs for the detection of salivary uric acid,[3] human serum albumin,[27] dopamine,[28] food pathogens,[29] and other biomarkers.[30] However, the development of a fully integrated device for direct real sample analysis remains a major bottleneck for μPADs to realize a lab-on-a-chip approach in point-of-care scenarios.

This study integrates μPADs with centrifugal microfluidic discs to realize the sample-in and answer-out POCT platform for salivary diagnostics. To evaluate the performance of this integrated device, the SARS-CoV-2 N protein is used as the model analyte. This centrifugal microfluidic disc is prepared by a commercial industry motor, a controller, and a charge supply to realize the saliva treatment. This μPAD was designed with sample zone, detection zone, control zone, and waste zone. NC membranes have a general negative electric charge in neutral and alkaline aqueous solutions.[31] The adsorption of proteins is caused mainly by multiple electrostatic attractions between the numerous permanent dipoles (the protein molecule). However, since the cellulose paper is synthesized by esterification with lots of hydroxylic groups on the surface, it is neutrally charged. Thus, it lacks the ability to immobilize proteins. Various reagents have been applied to treat the cellulosic paper surface to change their physicochemical properties, like chemical groups and surface charge, and to enhance their performances in biosensing.[22] Previously, the carboxylic acid group-terminated silica was used to fabricate the cellulosic paper, and the resultant μPAD was successfully used for the detection of hCG with a performance comparable to that of commercially available pregnancy test strips.[20] Poly-L-lysine (PLL), as a positively charged amino acid polymer, has a large relative molecular weight and a high density of positive charges, making it a desirable candidate to immobilize negatively charged macromolecular proteins based on the electrostatic interaction.[32] Being different from LFA in which the N protein antibody-labeled AuNP probes were deposited in the conjugation pad, herein, the probes are premixed with the sample before being added to the sample zone of μPADs. The capture antibody against N protein was immobilized on the PLL-treated detection zone, while the anti-IgG antibody was fixed on the PLL-treated control zone. In the presence of N protein, red color will develop on the test zone, and the color intensity can be quantified by the a portable colorimetric detector corresponding to the concentration of N-protein.

EXPERIMENTAL SECTION

Materials and Methods. Phosphate buffer saline tablets (Cat#P1000) and D-trehalose anhydrous (IT0870) were purchased from Solarbio (China). Sucrose (S112231-500g) and potassium carbonate were purchased from Aladdin (China). Polyvinylpyrrolidone (ST1614-50g) was obtained from Beyotime (China). Nov-PS-Ag6 N protein, COV19-PS-MAb2, and COV19-PS-MAb15 were obtained from Fapon Biotech (China). Goat antibody against mouse IgG (A102-Ab1) was purchased from Arton (China). Bovine serum albumin (B2063-50g), polyethylene glycol (PEG, 8210371000), tris(hydroxymethyl)aminomethane (T3253-250g), chloroauric acid, Nonidet P 40 (I3021-50 mL), proclin 300 (48912-U), poly-L-lysine (P5899-5 mg), Triton X-100 (93443-100 ML), and Tween20 (P9416-50 mL) were purchased from Sigma-Aldrich (United States). Grade 4 qualitative filter papers (Whatman, CAT No.1004-150), sample pad and conjugation pad (Kinbio, China, RB65), backing pad (Kinbio, China, SM31-25), and absorption pad (Kinbio, China, CH37) were used to make μPADs. Nitrocellulose membrane (JJ140) was purchased from Parabio (China). Instruments for making the LFA test strips include a guillotine cutter (ZQ2002) and dispenser (HM3035), which were purchased from Shanghai Kinbio Tech. Co.,

https://doi.org/10.1021/acssensors.3c01093
ACS Sens. 2023, 8, 3520−3529

Scheme 1. (a) Components of the Centrifugal Microfluidic Disc Including Three Layers of PMMA and Two Layers of PSA; (b) Photo of the Centrifugal Microfluidic Disc Integrated with μPADs; (c) Dimensions of the μPADs Assembled in the Centrifugal Microfluidic Disc; (d) Top View of the Configuration of 1st PMMA, 1st PSA, and 2nd PMMA; (e) Bottom View of the Configuration of 2nd PSA and 3rd PMMA; (f) Assay Process on μPADs for the Rapid Detection of Salivary SARS-COV-2 Nucleocapsid Protein

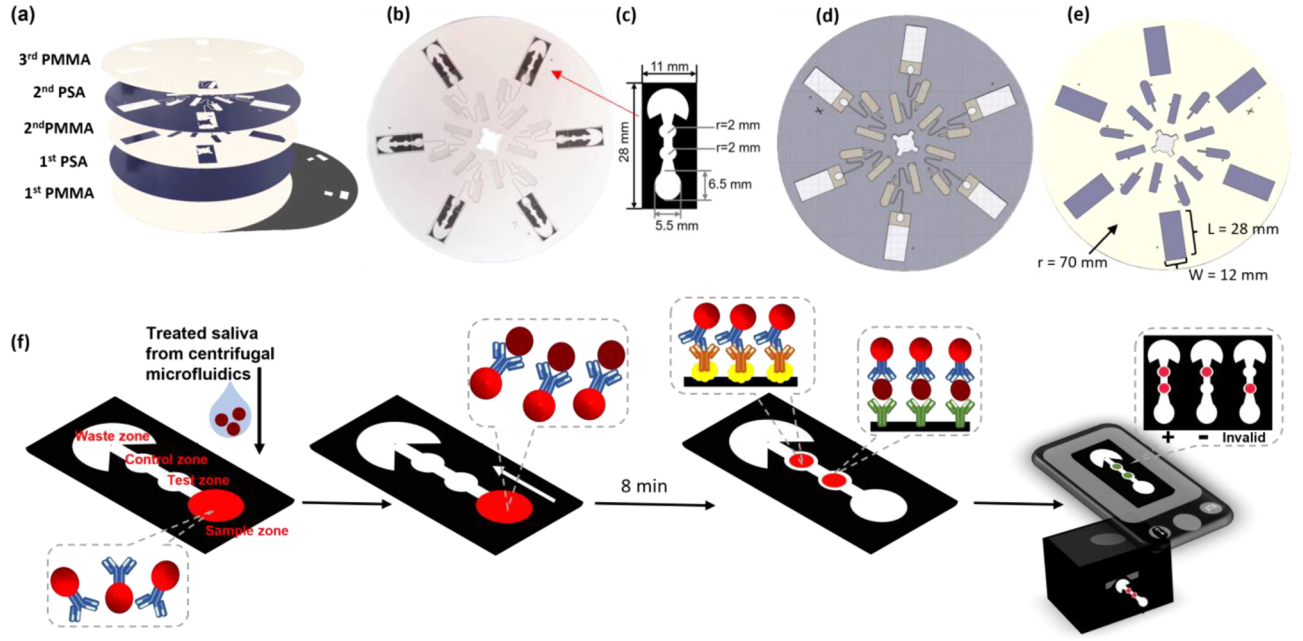

Ltd., China. UV−visible spectroscopy (UV-1900i, Shimadzu Co., Ltd., China) and scanning electron microscopy (FIB/SEM-TESCAN/SOLARIS GMH) were used to characterize the nanomaterials. SARS-CoV-2 pseudovirus and commercial YHLO SARS-CoV-2 N protein test strips were provided by Shenzhen YHLO Biotech.

Preparation of the AuNP Probes. The monodisperse suspension of AuNPs (40 nm) was prepared, referring to the bottom-up strategy.[33] The prepared AuNPs were stored at 4 °C before use. AuNPs were fetched out from the refrigerator in advance and dispersed in Milli-Q water. Potassium carbonate (0.25 M, 16 μL) was used to adjust the pH of the AuNP solution to 8.4. The anti-N-protein antibody CoV19-PS-MAb2 (15 μg) was added to the AuNP solution (1 mL) and incubated in the rotational incubator for 15 min. After incubation, a 1% BSA solution was applied to block the unbinding sites on AuNPs and incubated for another 15 min. The mixture was centrifuged at 4 °C for 15 min with 8000 rcf. The supernatant was discarded, and the AuNP probes were resuspended using the resuspension buffer (2 g of sucrose, 2 g of D-Trehalose anhydrous, 10 mg of PVP, 10 mg of BSA, 50 μL of Tween20, and 10 mL of 0.01 M PBS). The antibody-labeled AuNP probes were stored in 4 °C before usage.

Fabrication of the Centrifugal Microfluidic Motor System. The centrifugal microfluidic platform was built and modified with a commercial industry motor, controller, and charge supply (Figure S1). A brushless direct current motor (CAN&RS485) with a maximum rotation speed of 4500 rpm and the corresponding controller with an operation panel were purchased from BBMOTOR, China. The charge supply (S-250W-24 V) with an overload and short-circuit protection was purchased from PHLTD, China. A custom cross-shaped cap was 3D-printed by a Desktop 3D printer (Form3+, Formlab, USA) using resin (Black V4, Formlab) to adapt the disc to the motor spindle. Meanwhile, each disc layer was designed with the same cross-shaped center to fit the 3D-printed cap. The total cost of all parts was less than US$80 which was much cheaper than a centrifuge. To void turbulence during spinning, the motor was installed on an optical table by a custom fabricated steel rack. Alternatively, a custom desk clamp or a 3D-printed holder, which can be easily installed on the bench edge, can be developed to hold this motor for point-of-care detection. The safety shield was made of acrylic sheets.

Disc Manufacture and μPAD Integration. The microfluidic cartridges used in this study were assembled using multilayer lamination methods from three layers of poly(methyl methacrylate) (PMMA) and two layers of pressure-sensitive adhesive (PSA, Adhesives Research), as shown in Figure S2. The extruded part of the top layer PMMA was designed to clamp the μPADs. Considering the thickness difference, a spacer with a proper thickness was placed before inserting the μPADs to help hold the μPADs in place. Also, the spacer helped to cover the exposed adhesive PSA layer, making it easy to insert or remove the μPADs. All disc design (140 mm in diameter) was completed by Autodesk Fusion 360 software (Education License). The CO_2 laser (DY-33CO2, Dongying laser, China) was used to create features in both the PSA (126 μm thick) and PMMA (1.5 mm thick, 0.5 mm thick) layers, which resulted in microchannels and other small features. Large structures, such as reservoirs for reagent storage, were patterned in PMMA layers. These layers were aligned on a custom assembly tool kit. To achieve the most resistant bonding effect, 60 psi pressure was applied for 1 min by a hydraulic press (QYYLJ2023, Shunjie (Dongguan) Electromechanical Technology Co.) for strengthening the bond between the layers. The disc was constructed of five layers: (1) The base disc layer was a 1.5 mm thick PMMA layer to provide support to the chambers and reservoirs. (2) The second disc layer was a 126 μm thick PSA that serves as the bonding layer between the first layer PMMA and the second layer PSA. (3) Reagent chambers were configured on the 0.5 mm thick PMMA layer. (4) Microchannels connected to the main chambers by a siphon were fabricated on the second 126 μm thick PSA layer. (5) The top disc layer was a 1.5 mm thick PMMA layer with vent holes and sample collection reservoirs. Each sample collection reservoir was covered by an office tape and removed once the collection was completed. The sample collection reservoir only covered the sample-spotting area on μPAD, which enables μPAD to be removed easily for downstream readout in the dark box. The five layers were assembled, with the alignment realized by alignment holes. Six pieces of μPAD were inserted into the chamber in each unit reserved for embedding.

https://doi.org/10.1021/acssensors.3c01093
ACS Sens. 2023, 8, 3520−3529

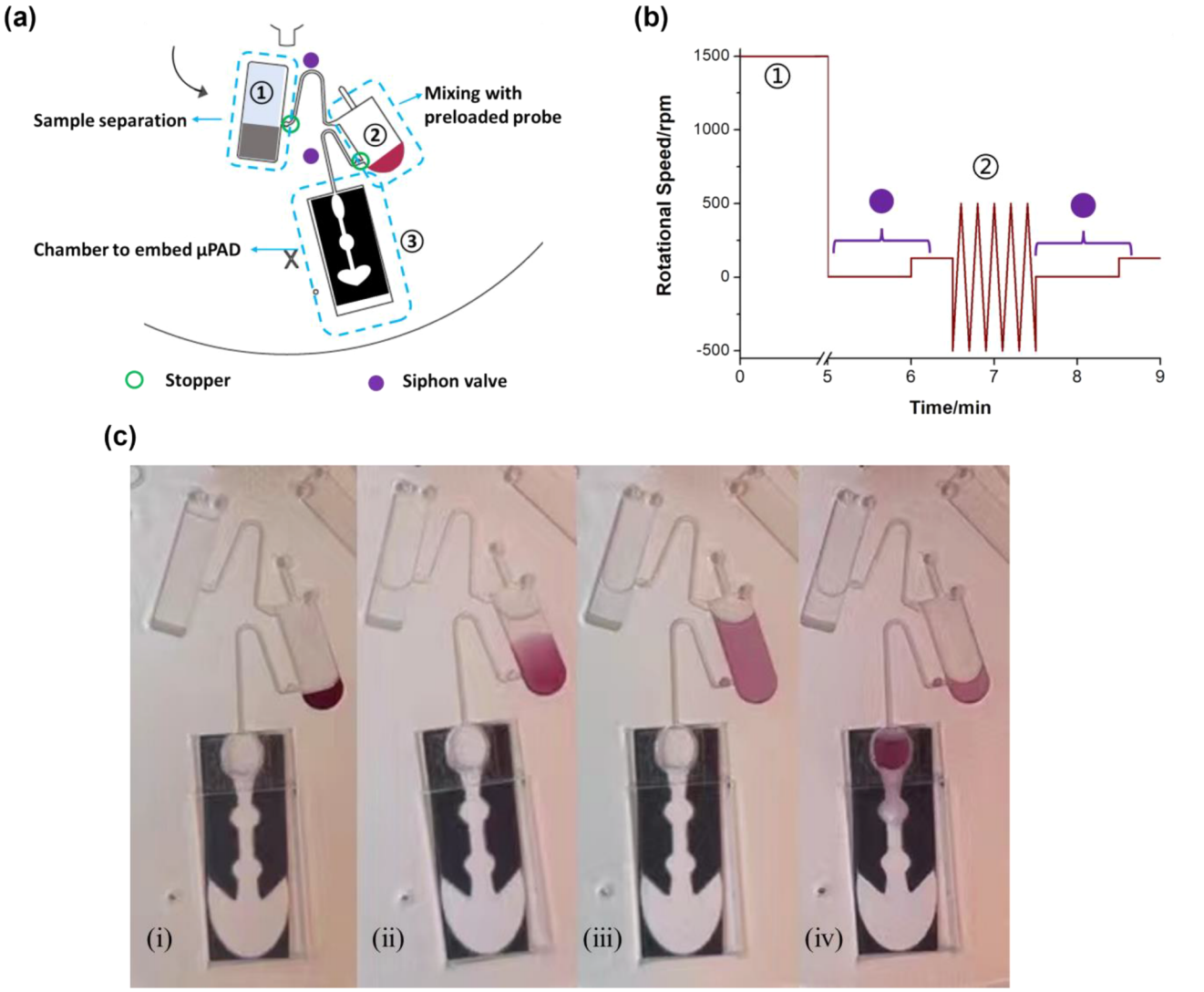

Figure 1. (a) Schematic diagram of on-disc saliva sample preparation procedures. (b) Time and rotation speed chart for on-disc operations, including sedimentation in chamber 1, the first siphon prime, sample transfer and mixing in chamber 2, the second siphon prime, product transfer, and product collection in chamber 3. (c) Photos for crucial on-disc steps including (i) precipitation, (ii) decanting, (iii) mixing, and (iv) sensing.

Fabrication of μPADs. μPADs were prepared by using a wax printer (Xerox ColorQube 8570) based on the structure and size in Scheme 1. A bottom circular area was prepared for sample loading, and the round shape and large area were suitable for liquid samples to flow along the channel. The small circles in the middle of the device were the test zone and control zone, respectively. The relatively smaller circle compared with the sample area was used for absolute reaction and concentrating the signal. The small circles in the straight channel provided a cushion for the liquid to guarantee the chemical to fully react with the capture antibody on the test zone and the control zone. The signal carried by antibody-labeled AuNP probes on the test zone and the control zone will concentrate in the area, providing visual signal readouts. The absorption area with the largest size was to ensure the sample to flow along the channel and pass through the test zone and the control zone. The shape of μPADs was optimized to the current design to ensure the good flow rate and efficiency. The wax was printed on #4 Whatman filter paper in the black area, forming hydrophobic boundaries after melting, confining the solution flow in the white region. After printing, the filter paper was heated at 120 °C for 4 min to melt the wax and let it soak into the filter paper, forming the hydrophobic boundaries. After heating, the printed cellulosic paper was stuck on the backing pad and stored in a dry and airtight bag for the next step.

Surface Modification of μPADs. To allow the sample to flow smoothly, the entire device was first run through a 15 μL of wetting buffer (0.01 M PBS, 0.01% Triton X-100) and incubated at 37 °C for 10 min. The test zone and the control zone were loaded with 0.3 μL of 0.0025% PLL in advance so that the capture antibody could be stabilized in the area. The PLL-treated cellulosic paper absorbed the capture antibody by the positive charge of the aminobutyl group. After loading PLL, the μPADs were incubated in an oven at 37 °C for 10 min to evaporate the water on μPADs, followed by the antibody attachment. COV19-PS-MAb15 (1.6 mg mL^{-1}, 0.3 μL) and goat antibody against mouse IgG (1.1 mg mL^{-1}, 0.3 μL) were added to the test zone and control zone, respectively; then μPAD was incubated in an oven at 37 °C for another 10 min. COV19-PS-MAb15 in the test zone could bind with the antibody-labeled AuNP probes carrying the antigen from the sample and display the signal of antigen concentration in the sample. The goat antibody against mouse IgG in the control zone could bind with the antigen-free AuNP probe, so that the signal in the control zone ensured the successful flow of the sample solution and functionality of the device. To reduce the nonspecific adsorption and improve the sensitivity of the assay, 15 μL of blocking buffer (2%BSA, 0.25%Tween20, 2%sucrose, 0.01 M PBS, pH 7.4) was added to the sample zone to screen out excess adsorption, followed by the incubation at 37 °C for 10 min.

https://doi.org/10.1021/acssensors.3c01093
ACS Sens. 2023, 8, 3520−3529

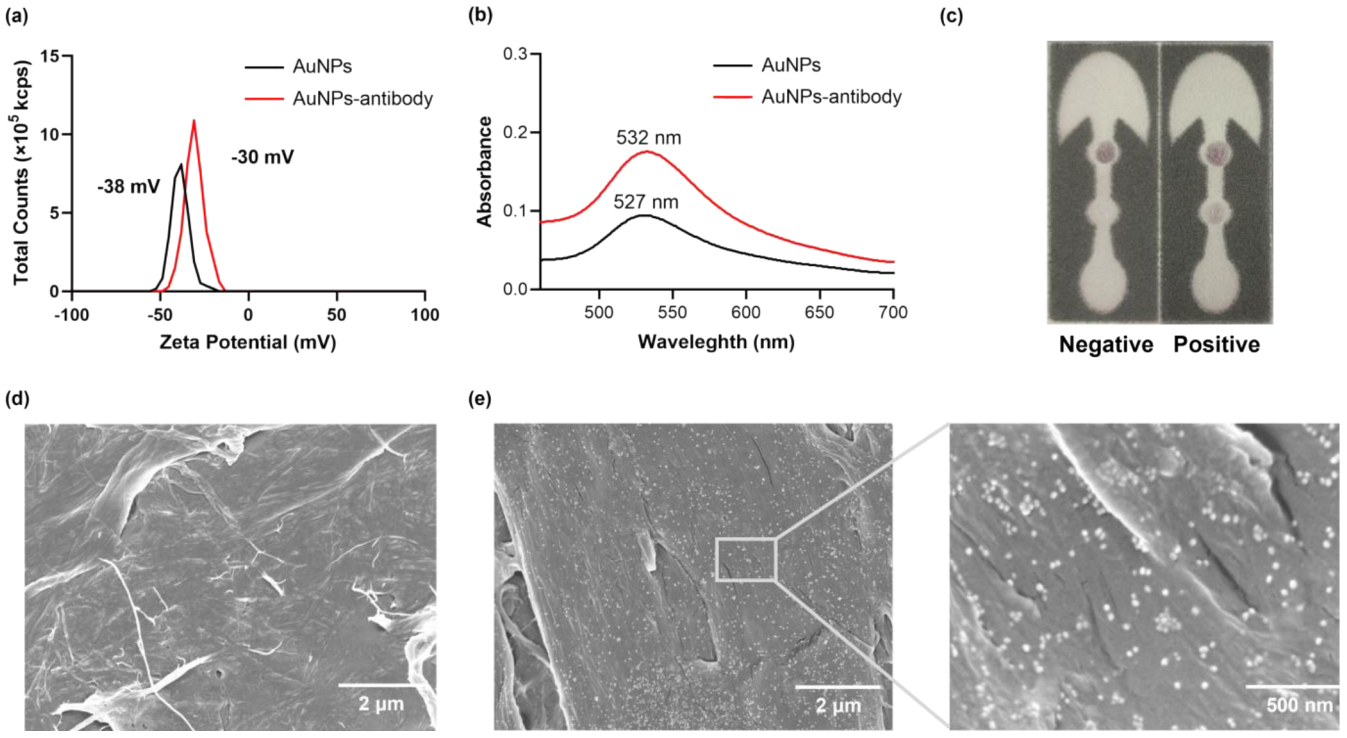

Figure 2. (a) Zeta potential measurement of the AuNPs. (b) UV−vis spectra of bare AuNPs and anti-N protein antibody-labeled AuNPs at different wavelengths. (c) Images of negative and positive on-disc μPADs. (d) SEM image of cellulosic paper at the detection zone of negative μPADs. (e) SEM images of cellulosic paper at the detection zone of positive μPADs in different magnifications.

Detection of SARS-CoV-2 N Protein. The AuNP probes were mixed with the antigen (SARS-CoV-2 N protein) solution in a ratio of 1:4. A mixture of 25 μL was loaded into the sample zone and then the solution flew to the adsorption pad. One of the binding sites of the N protein in the mixture bound to the antibodies of AuNP probes. When it flew to the test zone, another binding site on the N protein bound with MAb15 stabilized on the test zone. Higher amounts of N protein in the sample enabled more AuNP probes to stay on the test zone, and the red signal at the test zone was more intense. The red signal in the test zone was recorded by a smartphone in the black box 8 min after the sample solution was loaded. The color change was observed with the naked eyes, and the color intensity was analyzed by the software in the smartphone or ImageJ in the computer. All measurements were conducted at room temperature.

Detection of SARS-Cov-2 N Protein Spiked in Human Saliva. The developed device was used to quantify the N protein levels in human saliva samples collected by using the passive drooling method. The time for saliva collection was right after getting up in the morning and before brushing the teeth. The saliva was collected in front of the mouth; then, the head was tilted forward, and the saliva was collected into the tube to the marked level. The saliva samples were then stored at 4 °C until further use on the same day. Various concentrations of N protein in the phosphate buffer saline containing 0.025% SDS were spiked into saliva samples. The mixed solution was applied to the sample area of the μPADs, and after 8 min, the images of the μPADs were taken by a smartphone to quantify the optical signal on μPADs using ImageJ. The gray value was used as a signal indicator in the measurement.

Preparation of LFA Paper Test Strips. The sample pad of paper-based LFA test strips was treated with 0.01 M PBS (0.5% peg 2000, 5% sucrose, 1% BSA, 0.25% Tween-20, pH 7.4) and dried at 37 °C for 2 h. The conjugate pad was treated with 0.01 M PBS (10% sucrose, 0.25% Tween-20, 0.01% proclin 300, pH 7.4) and dried at 37 °C for 2 h. The NC membrane was assembled on the backplate. AuNP probes were dispensed on the treated conjugate pad at a rate of 5 μL cm^{-1} and subsequently baked at 37 °C for 2 h. Then, the goat antibodies against mouse IgG (1.1 mg mL^{-1}) and COV19-PS-MAb15 (1.2 mg mL^{-1}) were scribed on the NC membrane at 0.5 μL cm^{-1} to form the C line and T line, respectively, followed by drying at 37 °C for 2 h. Finally, the treated sample pad, conjugate pad, and absorption pad were assembled on the backplate, which was then cut into individual test strips with 4 mm width. The antigen solution (65 μL) was loaded on the sample pad, and the reading of LFA was taken after 15 min.

Design of a Smartphone-Adaptable Black Box. The black box (Figure S3) was printed on a 3D printer with the dimensions of 10 cm long, 15 cm wide, and 10 cm high. The front of the box has an 8 cm wide by 1 cm high drawer, to hold the μPAD, and an opening of 3 cm in diameter on the top for taking pictures by a smartphone.

RESULTS AND DISCUSSION

Characterization of the Centrifugal Microfluidic Disc with μPADs. Figure 1 shows the on-disc saliva sample preparation procedures. Before starting the rotation of the disc, 5 μL of AuNP probe solution was preloaded on chamber ②, and the saliva sample was loaded on chamber ① by a pipet. As shown in Figure 1b,c-i, the solid matrix in saliva formed sedimentation under centrifugation at 1500 rpm for 5 min. Then, the rotational speed was slowed down to 5 rpm to make the first siphon valve prime. The transfer of the supernatant in chamber ① occurred under a rotation speed of 130 rpm and was able to complete in 30 s. In chamber ②, the saliva supernatant was mixed with the preloaded AuNP probes under oscillation between −500 and 500 rpm for 3 min (Figure 1c-ii). The saliva samples (25 μL) were fully transferred to the small reservoir in chamber ③ in 30 s under a rotation speed of 130 rpm (Figure 1c-iii). After 8 min, the photo of the μPAD in Figure 1c-iv was taken in the black box for the concentration measurement.

Characterization of μPADs. The chromatic probe was prepared by adding COV19-PS-MAb2 to AuNPs (40 nm, 0.24

https://doi.org/10.1021/acssensors.3c01093
ACS Sens. 2023, 8, 3520−3529

nM) and then characterized using UV−vis spectroscopy and the zeta-potential value. The zeta potential of AuNPs was −38 mV due to the presence of negative charge at the surface.[34] The zeta potential of AuNPs after labeling with antibodies was −30 mV, which was consistent with that in the literature[35] (Figure 2a), suggesting the high stability of COV19-PS-MAb2-AuNPs conjugates.[36] Compared to the λ_{max} value for bare AuNPs at 527 nm, the λ_{max} value shifted to 532 nm after the binding of COV19-PS-MAb2 to AuNPs, which was consistent with that in the literature[37] (Figure 2b), suggesting the successful binding of antibodies on 40 nm AuNPs. Without the presence of the SARS-CoV-2 N protein in the sample, no antigen could bind with the AuNP probe and be captured by the antibody on the test zone. Further, no signal was present in the test zone. An obvious red signal would appear in the test zone in the presence of SARS-CoV-2 N protein in the sample (Figure 2c). Many AuNPs were distributed homogeneously on the filter paper surface, as shown in the SEM images (Figure 2e,f), demonstrating a sandwich immunosensor for N protein detection formed on the test zone.

Factors Affecting the Performance of the μPADs. To obtain the best chromatic signal from the μPADs, the effect of various parameters (such as the concentration of antibody-labeled AuNPs, concentration of antibodies deposited on the test line, and PLL concentration) on the color intensity of the test zone was optimized. The volume of the sample on μPADs and the ratio of AuNP probes to the antigen (N protein sample) were optimized. As shown in Figure 3a,b, the 25 μL sample in total containing the volume ratio of 1:4 (AuNP probes vs antigen) provided the highest signal. Therefore, we finally determined that AuNP probes were premixed with the antigen solution at a ratio of 1:4. A high concentration of PLL may lead to nonspecific binding of the probe to generate a false signal. A low concentration of PLL may lower the efficiency of antibody binding in the test zone and then influence the sensitivity negatively. Figure 3c shows the response of the μPADs treated with different concentrations of PLL (0.00125, 0.0025, 0.005, and 0.01%). The ratio of 0.0025% yielded the highest signal intensity, and therefore, it was chosen as the optimal value in this study.

COV19-PS-MAb2 at different concentrations (4, 8, 12, 15, and 20 μg mL^{-1}) was used for the preparation of AuNP probes (Figure 3d). The signal intensity (gray value) at a concentration of 15 μg mL^{-1} was similar to that of 20 μg mL^{-1}, as most of the probes were connected to the test zone and the control zone. Therefore, 15 μg mL^{-1} was considered the optimal COV19-PS-MAb2 concentration. In addition, μPADs with different concentrations of antibodies (0.4, 0.8, 1.2, 1.6, and 2 mg mL^{-1}) encapsulated on the test zone were prepared. The N protein samples (100 pg mL^{-1}) were then added to the prepared μPADs to study the effect of antibodies on the signal intensity. It was observed that 1.6 mg mL^{-1} provided roughly the same signal intensity as 2.0 mg mL^{-1} and was therefore used as the optimal concentration (Figure 3e). To find the optimal reading time for the analysis, 25 μL of sample containing 100 pg mL^{-1} N protein was applied to the μPADs, and readings were recorded using different time intervals (2, 4, 6, 8, 10, and 12 min). As shown in Figure 3f, the signal reached its highest value after 8 min, which was determined as the optimal reading time for analysis. In order to reduce the nonspecific adsorption and improve sensitivity, wetting buffer and blocking buffer were used for processing μPADs. It was obvious that after the wetting buffer and blocking buffer processing, the difference between 0 and 50 pg mL^{-1} gray values was much larger (Figure 3g,h). The signal-to-noise ratio of the experimental group was enhanced significantly compared to the control group.

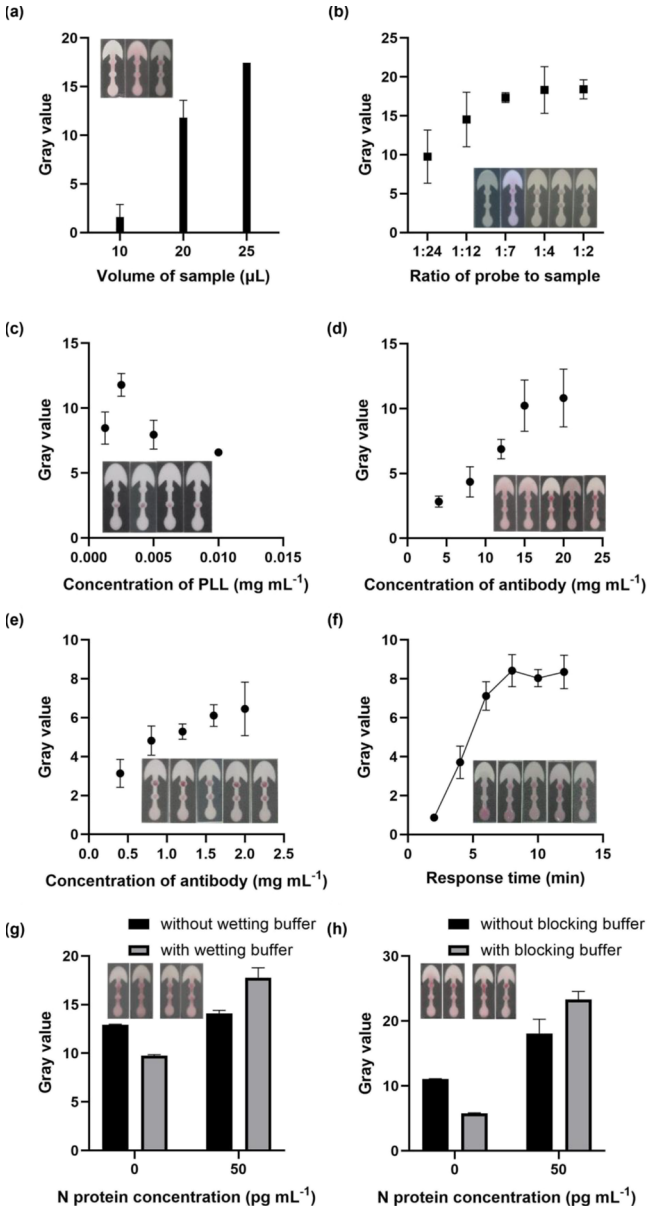

Figure 3. (a) Response of the device with different volumes of the sample on μPADs. (b) Response of the device with different ratios of probes to the antigen on μPADs. (c) Response of the device with different concentrations of PLL on μPADs. (d) Response of the device at various concentrations of antibody-labeled AuNP probes. (e) Response of the device at different concentrations of antibodies on the test zone of μPADs. (f) Assay time optimization. (g) Response of the device treated with or without the wetting buffer. (h) Response of the device treated with or without the blocking buffer (error bar is the standard deviation, $n = 3$).

Calibration Curve of SARS-Cov-2 N Protein Detection. After the N protein was loaded, the N protein bound to the AuNP probes according to the antigen and antibody interaction. The nanocomplex flew to the test zone and was captured by antibodies located in the test zone with the assistance of PLL. The N protein interacted with two types of antibodies by two different binding sites and formed a

https://doi.org/10.1021/acssensors.3c01093
ACS Sens. 2023, 8, 3520−3529

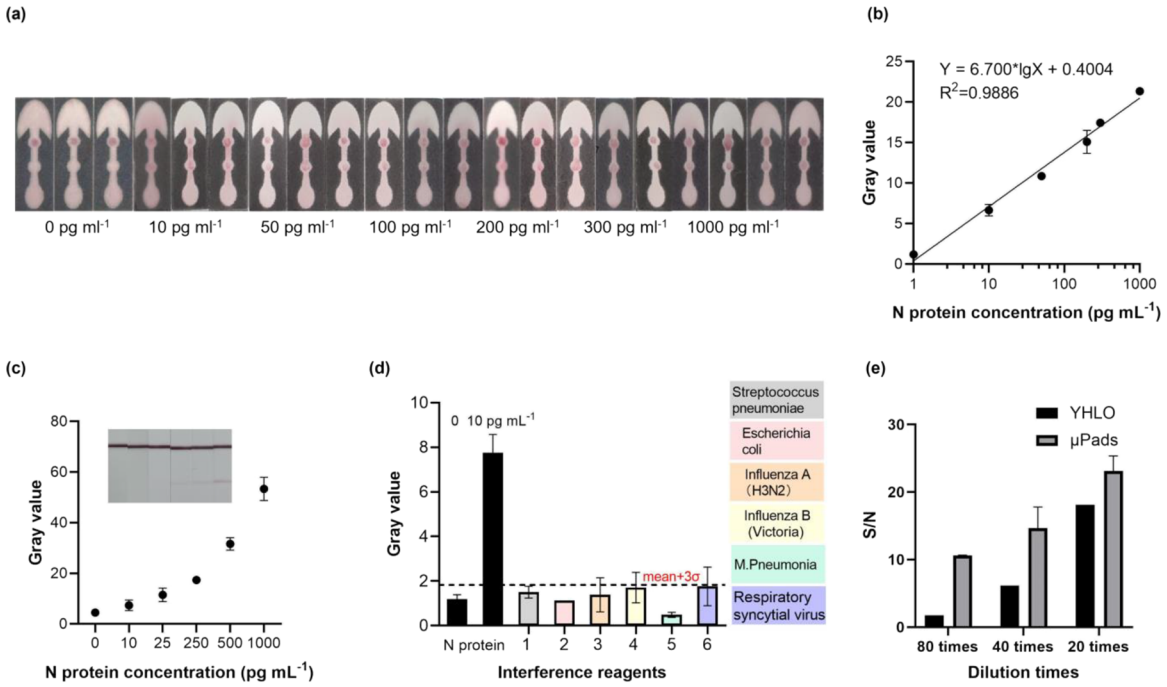

Figure 4. (a) Image of μPADs with different N protein concentrations. (b) Calibration curve for the detection of SARS-CoV-2 N protein with a linear range on μPADs (0−1000 pg mL^{-1}). (c) Calibration curve for the detection of SARS-CoV-2 N protein with a linear range on LFA (0−1000 pg mL^{-1}). (d) Response of the device under different interference reagents. (e) Comparison of the response of the device and commercial YHLO SARS-CoV-2 N protein test strips for the detection of pseudovirus (error bar is the standard deviation, n = 3).

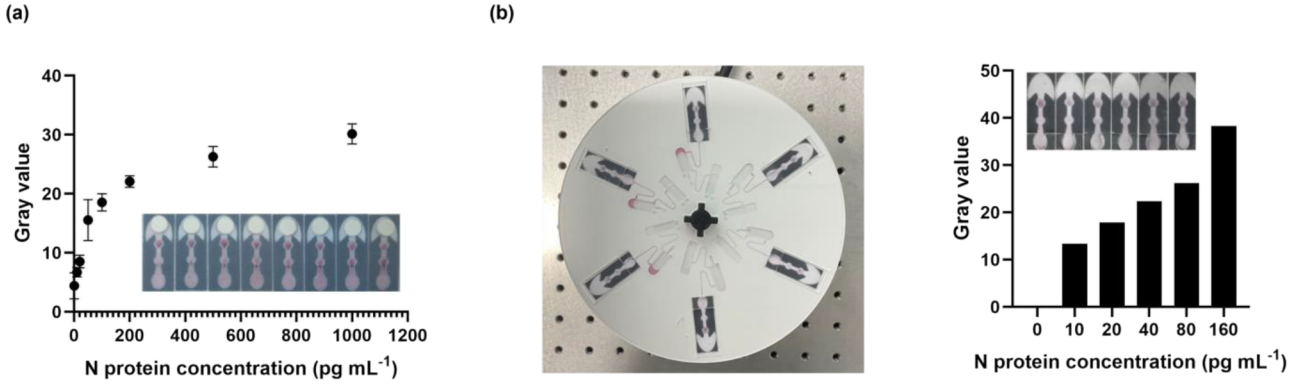

Figure 5. (a) Calibration curve of SARS-Cov-2 N protein spiked in saliva on μPADs with the adsorption pad on the waste zone (error bar is the standard deviation, n = 3). (b) Image of the centrifuge microfluidic disc with μPADs applied with SARS-Cov-2 N protein at different concentrations in saliva and the quantification results of six on-disc μPADs for the detection of SARS-Cov-2 N protein spiked in saliva.

sandwich structure. The red signal carried by AuNPs was displayed on the test zone with the sandwich structure nanocomposite, which was proportional to the amount of N protein in the sample. Different concentrations of N protein samples (0−1000 pg mL^{-1}) (25 μL) were added to the μPADs and incubated for 8 min to generate a calibration curve for the detection of SARS-CoV-2 N protein. After incubation, the μPADs were placed in the black box to obtain a photo, and the color intensity was analyzed by ImageJ. Figure 4a shows the images of μPADs for the detection of N proteins at different concentrations (0, 10, 50, 100, 200, 300, and 1000 pg mL^{-1}). The gray value increased with the concentration of N protein. The calibration curve demonstrated a clear positive proportional relationship between the concentration of N protein and the gray value, with the lowest detectable concentration of 10 pg mL^{-1} (Figure 4b), which is similar to that of LFA, indicating that the assay demonstrated similar detection performance to that of LFA (Figure 4c).

Specificity of the Integrated Device for the Detection of SARS-CoV-2 N Protein. To investigate the specificity of the on-disc μPADs, the device was tested in the presence of several interference reagents, such as *Streptococcus pneumoniae*, *Escherichia coli*, M pneumonia, respiratory syncytial virus, influenza virus A (H3N2), and influenza virus B (Victoria), respectively. The response of the device to different interference reagents is illustrated in Figure 4d, and it shows that the gray value of these signals generated by the interference reagents was much lower than that of the target analyte N protein (<mean of blank +3σ, σ is standard deviation). Most of the interference showed an almost negligible signal with respect to the signal of N protein. It

https://doi.org/10.1021/acssensors.3c01093
ACS Sens. 2023, 8, 3520−3529

suggests that the on-disc μPADs has a high specificity for the detection of SARS-CoV-2 N protein.

Validation of the Integrated Device by the Detection of Pseudovirus. To assess the validity of the on-disc μPADs for the detection of SARS-CoV-2 N protein, SARS-CoV-2 pseudovirus (20, 40, and 80 times dilution and blank control) (25 μL) was detected by the integrated device. The high ratio of signal-to-noise (S/N) indicates the functional validity of the device (Figure 4e). Compared with the commercial YHLO N protein test strips, μPADs showed a high degree of differentiation from the blank control (Figure 4e). The device could differentiate the SARS-CoV-2-inactivated virus and present a color gradient with respect to the virus concentration difference.

Calibration Curve of SARS-CoV-2 N Protein Detection in Saliva. To assess the practicality and accuracy of the prepared colorimetric LFA test strips, different concentrations of N protein (0, 10, 20, 50, 100, 200, 500, and 1000 pg mL^{-1}) were added to the negative saliva, and the levels were then measured (Figure 5a). Saliva contains protein and many ions that make it very viscous.[38] To demonstrate the efficacy of the developed centrifugal microfluidic disc for saliva treatment, the μPADs without being assembled on the disc were used to study the flow of AuNP probes after adding saliva samples in different dilutions (Figure S4a). It was observed that AuNP probes after the addition of 100% saliva sample without N protein could not move along μPADs and could move smoothly with 25% saliva sample with the aid of an adsorption pad in the waste zone. However, a significant nonspecific adsorption was observed. However, 25% saliva containing 0.025% SDS could reduce specific adsorption while maintaining a smooth flow on μPADs (Figure S4b). However, upon removing the absorption pad from the μPADs, the flow of the sample slows down, and nonspecific adsorption reoccurred in the test zone, leading to a noticeable decrease in sensitivity (Figure S4c). Thus, the additional adsorption pad and 0.025% SDS together were able to decrease the nonspecific adsorption on μPADs without the aid of a centrifugal microfluidic disc. In order to realize the POCT, saliva treatment, addition of AuNP probes, and automated mixing were combined to the centrifuge microfluidic disc with μPADs (Figure 5b). Different concentrations of the SARS-COV-2 N protein in saliva (0, 10, 20, 40, 80, and 160 pg mL^{-1}) were tested on the centrifugal microfluidic disc with μPADs. As shown in Figure 5b, nonspecific adsorption was not observed on on-disc μPADs, and the saliva flew smoothly without the addition of the additional adsorption pad in the waste zone. A similar sensitivity (10 pg mL^{-1}) was achieved to that based on N protein in PBS solution. The performance of the device is compared with other methods for the detection of SARS-CoV-2 N protein (Table S1). The integrated device shows the shortest assay time while providing noninvasive POCT in a sample-in-answer-out fashion. Saliva is treated as a mirror of our body health, and thus the detection of biomarker in saliva is essential in disease diagnosis. Saliva volume and biochemical composition differ among individuals; these parameters are influenced by age,[39] sex,[40] and diet.[41] Thus, salivary sample handling criteria need to be standardized. To obtain an accurate and reliable comparison of salivary analysis in different laboratories, the time point of saliva collection and other factors need to be specified.[42] To minimize variables, a fixed method of saliva collection was used in this study, and the effect of different factors on salivary diagnostics will be reported in our next study.

CONCLUSIONS

Development of an integrated point-of-care device with the function of both sample treatment and analysis is critical for providing an overall strategy to control the COVID-19 pandemic or other contagious diseases with assured quality, safety, affordability, and performance. Considering the high cost and environment concerns of the NC membrane used in a LFA, which is the main type of POCT device for early disease diagnosis, we developed the cellulosic paper-based μPADs which were integrated with a centrifugal microfluidic disc system to enable rapid and efficient salivary daignostics. μPADs as the second generation of LFA, replaced the NC membrane with cellulosic paper to realize the comparable sensitivity but with low cost and short assay time. Semi-quantitative measurement by the analysis of the colorimetric signal on the μPADs can be performed by accompanying a black box and the smartphone photography with the lowest detection limit of 10 pg mL^{-1}. The integrated device was specific to the detection of SARS-COV-2 N protein and showed comparable performance to that of commercial LFA test strips using the SARS-CoV-2 pseudovirus. Combining the centrifugal microfluidic disc with the μPADs allows saliva to be processed and tested for sample-in-answer-out results. This fully integrated device for saliva treatment and analysis provides massive potentials in noninvasive POCT for early screening of contagious diseases, especially in the resource-limited settings.

ASSOCIATED CONTENT

Supporting Information

The Supporting Information is available free of charge at https://pubs.acs.org/doi/10.1021/acssensors.3c01093.

Components of the centrifugal microfluidic platform including motor, controller and charge supply; schematic of the integration procedures of μPADs to the centrifuge microfluidic disc; picture of the black box for smartphone signal readout; images of off-disc μPADs with and without adsorption pads in the waste zone, responding to different saliva samples; and comparison of the different immunoassays for the detection of SARS-CoV-2 N protein (PDF)

AUTHOR INFORMATION

Corresponding Author

Guozhen Liu − *CUHK(SZ)-Boyalife Joint Laboratory of Regenerative Medicine Engineering, School of Medicine, The Chinese University of Hong Kong, Shenzhen 518172, China; Ciechanover Institute of Precision and Regenerative Medicine, School of Medicine, The Chinese University of Hong Kong, Shenzhen 518172, China;* orcid.org/0000-0002-0556-6404; Email: liuguozhen@cuhk.edu.cn

Authors

Shixian Liu − *CUHK(SZ)-Boyalife Joint Laboratory of Regenerative Medicine Engineering, School of Medicine, The Chinese University of Hong Kong, Shenzhen 518172, China; Ciechanover Institute of Precision and Regenerative Medicine, School of Medicine, The Chinese University of Hong Kong, Shenzhen 518172, China*

https://doi.org/10.1021/acssensors.3c01093
ACS Sens. 2023, 8, 3520−3529

Yuting Hou − *CUHK(SZ)-Boyalife Joint Laboratory of Regenerative Medicine Engineering, School of Medicine, The Chinese University of Hong Kong, Shenzhen 518172, China; Ciechanover Institute of Precision and Regenerative Medicine, School of Medicine, The Chinese University of Hong Kong, Shenzhen 518172, China*

Zirui Li − *CUHK(SZ)-Boyalife Joint Laboratory of Regenerative Medicine Engineering, School of Medicine, The Chinese University of Hong Kong, Shenzhen 518172, China; Ciechanover Institute of Precision and Regenerative Medicine, School of Medicine, The Chinese University of Hong Kong, Shenzhen 518172, China*

Chenyu Yang − *CUHK(SZ)-Boyalife Joint Laboratory of Regenerative Medicine Engineering, School of Medicine, The Chinese University of Hong Kong, Shenzhen 518172, China; Ciechanover Institute of Precision and Regenerative Medicine, School of Medicine, The Chinese University of Hong Kong, Shenzhen 518172, China*

Complete contact information is available at: https://pubs.acs.org/10.1021/acssensors.3c01093

Notes

The authors declare no competing financial interest.

■ ACKNOWLEDGMENTS

The work was financially supported by the National Natural Science Foundation of China (grant nos. 22174121, 22211530067, and T2250710180), 2022 Natural Science Foundation of Guangdong Provincial Basic and Applied Basic Research Fund (Guangdong Hybribio), Shenzhen Bay Open Laboratory Fund 2021 by Shenzhen Bay Laboratory, CUHK(SZ)—Boyalife Joint Laboratory of Regenerative Medicine Engineering Fund, CUHK(SZ)—The Second Affiliated Hospital Joint Fund YXLH2205, and the University Development Fund (UDF01002012). Shenzhen YHLO Biotech is acknowledged for providing SARS-CoV-2 pseudovirus and commercial YHLO SARS-CoV-2 N protein test strips for this study.

■ REFERENCES

(1) Ngamchuea, K.; Chaisiwamongkhol, K.; Batchelor-McAuley, C.; Compton, R. G. Chemical analysis in saliva and the search for salivary biomarkers − a tutorial review. *Analyst* **2018**, *143* (1), 81−99.

(2) Gug, I. T.; Tertis, M.; Hosu, O.; Cristea, C. Salivary biomarkers detection: Analytical and immunological methods overview. *TrAC, Trends Anal. Chem.* **2019**, *113*, 301−316.

(3) Fan, K.; Zeng, J.; Yang, C.; Wang, G.; Lian, K.; Zhou, X.; Deng, Y.; Liu, G. Digital quantification method for sensitive point-of-care detection of salivary uric acid using smartphone-assisted μPADs. *ACS Sens.* **2022**, *7* (7), 2049−2057.

(4) Bodur, S.; Erarpat, S.; Günkara, Ö. T.; Bakirdere, S. Accurate and sensitive determination of hydroxychloroquine sulfate used on COVID-19 patients in human urine, serum and saliva samples by GC-MS. *J. Pharm. Anal.* **2021**, *11* (3), 278−283.

(5) Fabiani, L.; Saroglia, M.; Galatà, G.; De Santis, R.; Fillo, S.; Luca, V.; Faggioni, G.; D'Amore, N.; Regalbuto, E.; Salvatori, P.; Terova, G.; Moscone, D.; Lista, F.; Arduini, F. Magnetic beads combined with carbon black-based screen-printed electrodes for COVID-19: A reliable and miniaturized electrochemical immunosensor for SARS-CoV-2 detection in saliva. *Biosens. Bioelectron.* **2021**, *171*, No. 112686.

(6) Johannsen, B.; Müller, L.; Baumgartner, D.; Karkossa, L.; Früh, S. M.; Bostanci, N.; Karpíšek, M.; Zengerle, R.; Paust, N.; Mitsakakis, K. J. M. Automated pre-analytic processing of whole saliva using magnet-beating for point-of-care protein biomarker analysis. *Micromachines* **2019**, *10* (12), 833.

(7) Jiang, K.; Jokhun, D. S.; Lim, C. T. Microfluidic detection of human diseases: From liquid biopsy to COVID-19 diagnosis. *J. Biomech.* **2021**, *117*, No. 110235.

(8) Michael, I. J.; Kim, T.-H.; Sunkara, V.; Cho, Y.-K. Challenges and opportunities of centrifugal microfluidics for extreme point-of-care testing. *Micromachines* **2016**, *7*, 32.

(9) Zhao, Y.; Hou, Y.; Ji, J.; Khan, F.; Thundat, T.; Harrison, D. J. Sample preparation in centrifugal microfluidic discs for human serum metabolite analysis by surface assisted laser desorption/ionization mass spectrometry. *Anal. Chem.* **2019**, *91* (12), 7570−7577.

(10) Malic, L.; Brassard, D.; Da Fonte, D.; Nassif, C.; Mounier, M.; Ponton, A.; Geissler, M.; Shiu, M.; Morton, K. J.; Veres, T. Automated sample-to-answer centrifugal microfluidic system for rapid molecular diagnostics of SARS-CoV-2. *Lab Chip* **2022**, *22* (17), 3157−3171.

(11) Turiello, R.; Dignan, L. M.; Thompson, B.; Poulter, M.; Hickey, J.; Chapman, J.; Landers, J. P. Centrifugal microfluidic method for enrichment and enzymatic extraction of severe acute respiratory syndrome coronavirus 2 RNA. *Anal. Chem.* **2022**, *94* (7), 3287−3295.

(12) Johannsen, B.; Müller, L.; Baumgartner, D.; Karkossa, L.; Früh, S. M.; Bostanci, N.; Karpíšek, M.; Zengerle, R.; Paust, N.; Mitsakakis, K. Automated pre-analytic processing of whole saliva using magnet-beating for point-of-care protein biomarker analysis. *Micromachines* **2019**, *10*, 833.

(13) Li, T.; Wang, L.; Wang, H.; Li, X.; Zhang, S.; Xu, Y.; Wei, W. Serum SARS-COV-2 nucleocapsid protein: a sensitivity and specificity early diagnostic marker for SARS-COV-2 infection. *Front. Cell. Infect. Microbiol.* **2020**, *10*, 470.

(14) Benzigar, M. R.; Bhattacharjee, R.; Baharfar, M.; Liu, G. Current methods for diagnosis of human coronaviruses: pros and cons. *Anal. Bioanal. Chem.* **2021**, *413* (9), 2311−2330.

(15) Corman, V. M.; Landt, O.; Kaiser, M.; Molenkamp, R.; Meijer, A.; Chu, D. K.; Bleicker, T.; Brünink, S.; Schneider, J.; Schmidt, M. L. Detection of 2019 Novel Coronavirus (2019-nCoV) by real-time RT-PCR. *Euro Surveill.* **2020**, *25* (3), No. 2000045.

(16) Peeling, R. W.; Heymann, D. L.; Teo, Y.-Y.; Garcia, P. J. Diagnostics for COVID-19: moving from pandemic response to control. *Lancet* **2021**, *21*, 1334 DOI: 10.1016/S1473-3099(21)00291-7.

(17) Sri Santosh, T.; Parmar, R.; Anand, H.; Srikanth, K.; Saritha, M. A review of salivary diagnostics and its potential implication in detection of Covid-19. *Cureus* **2020**, *12* (4), No. e7708.

(18) Shirshahi, V.; Liu, G. Enhancing the analytical performance of paper lateral flow assays: From chemistry to engineering. *TrAC, Trends Anal. Chem.* **2021**, *136*, No. 116200.

(19) Peto, T.; Affron, D.; Afrough, B.; Agasu, A.; Ainsworth, M.; Allanson, A.; Allen, K.; Allen, C.; Archer, L.; Ashbridge, N. COVID-19: Rapid antigen detection for SARS-CoV-2 by lateral flow assay: A national systematic evaluation of sensitivity and specificity for mass-testing. *EClinicalMedicine* **2021**, *36*, No. 100924.

(20) Rahbar, M.; Zou, S.; Baharfar, M.; Liu, G. A customized microfluidic paper-based platform for colorimetric immunosensing: Demonstrated via hcg assay for pregnancy test. *Biosensors* **2021**, *11* (12), 474.

(21) Singh, A. T.; Lantigua, D.; Meka, A.; Taing, S.; Pandher, M.; Camci-Unal, G. Paper-based sensors: Emerging themes and applications. *Sensors* **2018**, *18* (9), 2838.

(22) Liu, Y.; Lu, S.; Zhang, Z.; Yang, Z.; Cui, X.; Liu, G. Printable biosensors towards next-generation point-of-care testing: paper substrate as an example. *Lab Chip* **2023**, *23* (15), 3328−3352.

(23) Noviana, E.; Ozer, T.; Carrell, C. S.; Link, J. S.; McMahon, C.; Jang, I.; Henry, C. S. Microfluidic paper-based analytical devices: From design to applications. *Chem. Rev.* **2021**, *121* (19), 11835−11885.

(24) Amor-Gutiérrez, O.; Rama, E. C.; Costa-García, A.; Fernández-Abedul, M. T. based maskless enzymatic sensor for glucose

determination combining ink and wire electrodes. *Biosens. Bioelectron.* **2017**, *93*, 40−45.
(25) Baharfar, M.; Rahbar, M.; Tajik, M.; Liu, G. Engineering strategies for enhancing the performance of electrochemical paper-based analytical devices. *Biosens. Bioelectron.* **2020**, *167*, No. 112506.
(26) Ge, S.; Zhang, L.; Zhang, Y.; Lan, F.; Yan, M.; Yu, J. Nanomaterials-modified cellulose paper as a platform for biosensing applications. *Nanoscale* **2017**, *9* (13), 4366−4382.
(27) Luo, Z.; Lv, T.; Zhu, K.; Li, Y.; Wang, L.; Gooding, J. J.; Liu, G.; Liu, B. Paper-based ratiometric fluorescence analytical devices towards point-of-care testing of human serum albumin. *Angew. Chem., Int. Ed.* **2020**, *59* (8), 3131−3136.
(28) Baharfar, M.; Mayyas, M.; Rahbar, M.; Allioux, F.-M.; Tang, J.; Wang, Y.; Cao, Z.; Centurion, F.; Jalili, R.; Liu, G.; Kalantar-Zadeh, K. Exploring interfacial graphene oxide reduction by liquid metals: Application in selective biosensing. *ACS Nano* **2021**, *15* (12), 19661−19671.
(29) Zhuang, J.; Zhao, Z.; Lian, K.; Yin, L.; Wang, J.; Man, S.; Liu, G.; Ma, L. SERS-based CRISPR/Cas assay on microfluidic paper analytical devices for supersensitive detection of pathogenic bacteria in foods. *Biosens. Bioelectron.* **2022**, *207*, No. 114167.
(30) Liu, S.; Shen, Z.; Deng, L.; Liu, G. Smartphone assisted portable biochip for non-invasive simultaneous monitoring of glucose and insulin towards precise diagnosis of prediabetes/diabetes. *Biosens. Bioelectron.* **2022**, *209*, No. 114251.
(31) Přistoupil, T.; Kramlová, M.; Štěrbíková, J. On the mechanism of adsorption of proteins to nitrocellulose in membrane chromatography. *J. Chromatogr. A* **1969**, *42*, 367−375.
(32) Stearns, N. A.; Zhou, S.; Petri, M.; Binder, S. R.; Pisetsky, D. S. The use of poly-L-lysine as a capture agent to enhance the detection of antinuclear antibodies by ELISA. *PloS one* **2016**, *11* (9), No. e0161818.
(33) Zhao, L.; Jiang, D.; Cai, Y.; Ji, X.; Xie, R.; Yang, W. Tuning the size of gold nanoparticles in the citrate reduction by chloride ions. *Nanoscale* **2012**, *4* (16), 5071−5076.
(34) Tabrizi, A.; Ayhan, F.; Ayhan, H. Gold nanoparticle synthesis and characterisation. *Hacettepe J. Biol. Chem.* **2009**, *37* (3), 217−226.
(35) Wangoo, N.; Kaushal, J.; Bhasin, K. K.; Mehta, S. K.; Suri, C. R. Zeta potential based colorimetric immunoassay for the direct detection of diabetic marker HbA1c using gold nanoprobes. *Chem. Commun.* **2010**, *46* (31), 5755−5757.
(36) Majzik, A.; Patakfalvi, R.; Hornok, V.; Díkány, I. Growing and stability of gold nanoparticles and their functionalization by cysteine. *Gold Bull.* **2009**, *42* (2), 113−123.
(37) Hou, W.; Wang, S.; Wang, X.; Han, X.; Fan, H.; Cao, S.; Yue, J.; Wang, Q.; Jiang, W.; Ding, C.; Yu, S. Development of colloidal gold immunochromatographic strips for detection of riemerella anatipestifer. *PLoS One* **2015**, *10* (3), No. e0122952.
(38) Carpenter, G. H. The secretion, components, and properties of saliva. *Annu. Rev. Food Sci. Technol.* **2013**, *4* (1), 267−276.
(39) Arhakis, A.; Karagiannis, V.; Kalfas, S. Salivary alpha-amylase activity and salivary flow rate in young adults. *Open Dent. J.* **2013**, *7*, 7−15.
(40) Lukacs, J. R.; Largaespada, L. L. Explaining sex differences in dental caries prevalence: saliva, hormones, and "life-history" etiologies. *Am. J. Hum. Biol.* **2006**, *18* (4), 540−55.
(41) Dawes, C. Effects of diet on salivary secretion and composition. *J. Dent. Res.* **1970**, *49* (6), 1263−73.
(42) Bhattarai, K. R.; Kim, H. R.; Chae, H. J. Compliance with saliva collection protocol in healthy volunteers: Strategies for managing risk and errors. *Int. J. Med. Sci.* **2018**, *15* (8), 823−831.

https://doi.org/10.1021/acssensors.3c01093
ACS Sens. 2023, 8, 3520−3529